

Supplementary Materials

Mechanically-Controlled Reversible Binary Conductance Switching of a Single-Molecule Junction

Su Ying Quek¹, Maria Kamenetska^{2,3}, Michael L. Steigerwald⁴, Hyoung Joon Choi⁵, Steven G. Louie^{1,6}, Mark S. Hybertsen⁷, J. B. Neaton¹, L. Venkataraman^{2,3}

¹Molecular Foundry, Lawrence Berkeley National Laboratory, Berkeley, CA

²Department of Applied Physics, Columbia University, New York, NY

³Center for Electron Transport in Nanostructures, Columbia University, New York, NY

⁴Department of Chemistry, Columbia University, New York, NY

⁵Department of Physics and IPAP, Yonsei University, Seoul, Korea

⁶Department of Physics, University of California, Berkeley, Berkeley, CA

⁷Center for Functional Nanomaterials, Brookhaven National Laboratory, Upton, NY

Contents

1. Experimental Details and Controls

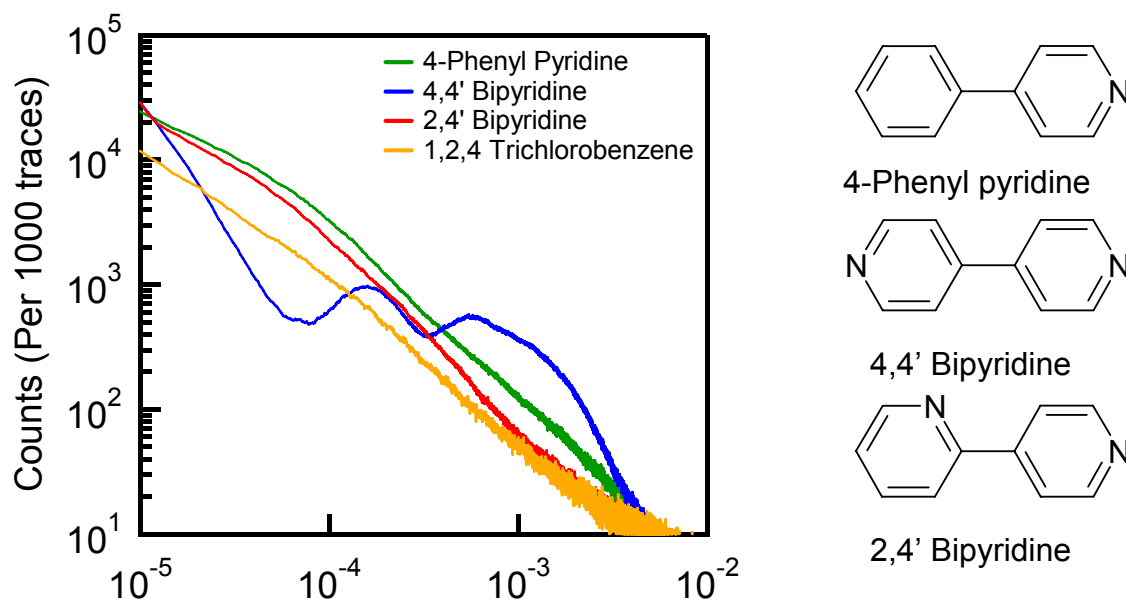
2. Theoretical Methods

3. Discussion of Alternative Explanations for High G and Low G Configurations

Experimental Details and Controls:

Experimental Setup and Procedures: The details of our experimental apparatus has been described previously^{1, 2}. Briefly, the STM was constructed from a home-built tip holder mounted on top of a single-axis piezoelectric positioner with built-in position sensor (Mad City Labs). A bias was applied between a cut Au wire tip and a Au substrate placed on top of the piezoelectric positioner and the resulting current was converted to a voltage with a current amplifier (Keithley 428). Data collection and control of the piezoelectric positioner were done by means of a data acquisition board (National Instruments, PXI-4461) driven by a customized program using Igor software (Wavemetrics Inc.) For the conductance trace measurements, the substrate approached the tip until a set conductance larger than G_0 was measured to ensure that the Au/molecule/Au junction from the previous measurement was completely destroyed. For standard conductance measurements, the sample was then withdrawn at a rate of 16 nm/s and the current and position data was recorded at a 40 kHz sampling frequency. Histograms were constructed from the current versus position traces by dividing the current by measured voltage across the junction to obtain conductances and then binning the data as a function of conductance, without selecting any traces. SI Figure 1 shows conductance histograms for three molecules; 4-phenyl pyridine (Sigma-Aldrich), 4,4' bipyridine (Sigma-Aldrich) and 2,4' bipyridine (Alfa-Aesar) measured in solvent 1,2,4 trichlorobenzene (Sigma-Aldrich).

All position determinations were based on measurements with a built-in position sensor within our custom piezoelectric positioner. This position sensor was calibrated both by the manufacturer and by us using laser interference measurements. We found the absolute values of the measured displacements to be accurate to within 5%.



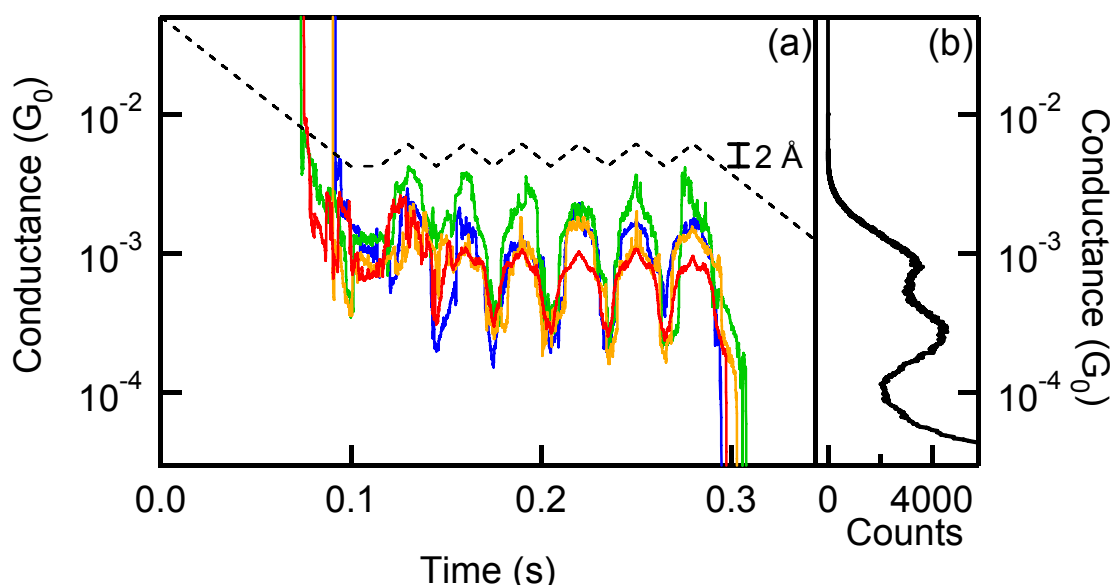
SI Fig. 1: Conductance histograms for 4-phenyl pyridine, 4,4' bipyridine, 2,4' bipyridine and in solvent alone (1,2,4 trichlorobenzene), and chemical structures for all molecules. All histograms computed from 10000 traces individual traces without any data selection or processing using a linear bin size of $10^{-6} G_0$.

Step Detection Algorithm: The molecular junction step detection was carried out as follows. First, a Lorentzian was fit to the histograms computed from all measured traces to determine the Low G and High G ranges (conductance peak position (G_{peak}) and the full width at half maximum for the peak (G_{width})). For each measured trace, the derivative of the logarithm of the trace was computed. Traces with peaks in the derivative that crossed a threshold of 5000 were considered further. The average conductance from the raw data in the region between two successive peaks was computed. Traces were considered to have molecular steps if this average conductance was within $G_{\text{peak}} \pm G_{\text{width}}$ and if this region had more than 5 data points. Steps that had fewer than 5 data points, or equivalently those that were shorter than 0.007 nm were not included in the analysis.

A detailed statistical analysis of individual traces using this automated step detection algorithm showed that 95 % of the measured traces had a High G step and that 75% had a

Low G step. While a significant fraction ($\sim 20\%$) of the measured traces had only a High G step, there were virtually no traces (under 3%) that had only a Low G step, consistent with the lack of counts at the origin of Fig. 1c in the Low G range.

Analysis of Switching Traces: Switching traces were selected from all measured traces using an automated algorithm. The number of data points in the initial "hold" region of each trace that had a conductance within the Low G range was determined. If more than 75% of the data was within this conductance range, the trace was selected. Typically, 10% of all measured switching traces in 4,4' bipyridine were selected. A histogram using $10^{-6} G_0$ bin size was constructed from these selected traces using data collected during the switching section of the ramp.

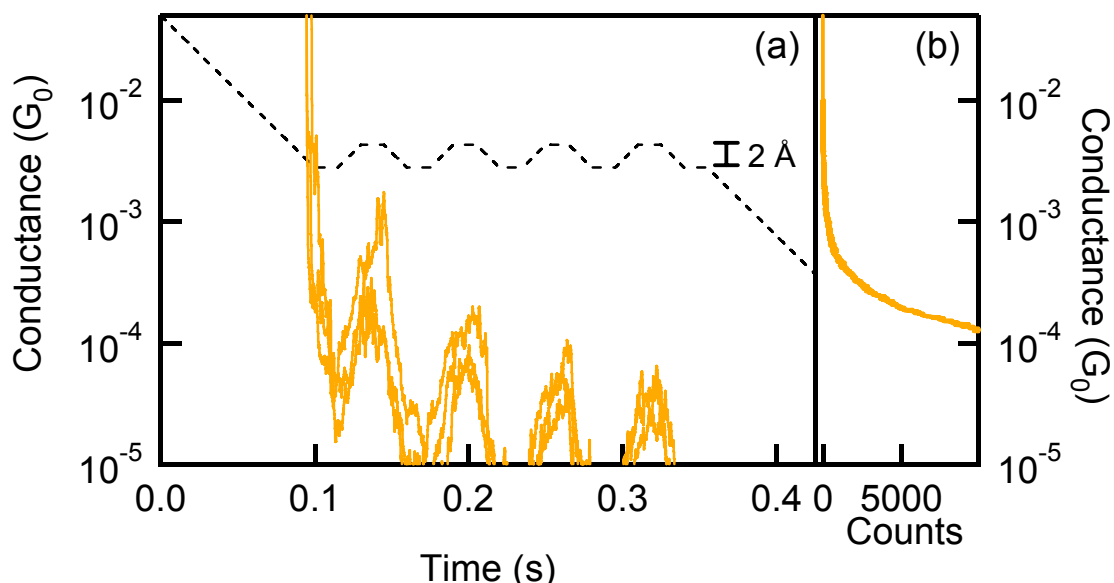


SI Fig. 2: (a) Sample switching traces measured with a zig-zag ramp (dashed line) with 4,4' bipyridine showing switching six times between the Low G and High G conductance. (b) Conductance histogram constructed from 860 selected traces out of 9000 measured traces. Measurements were carried out with a 250 mV applied bias.

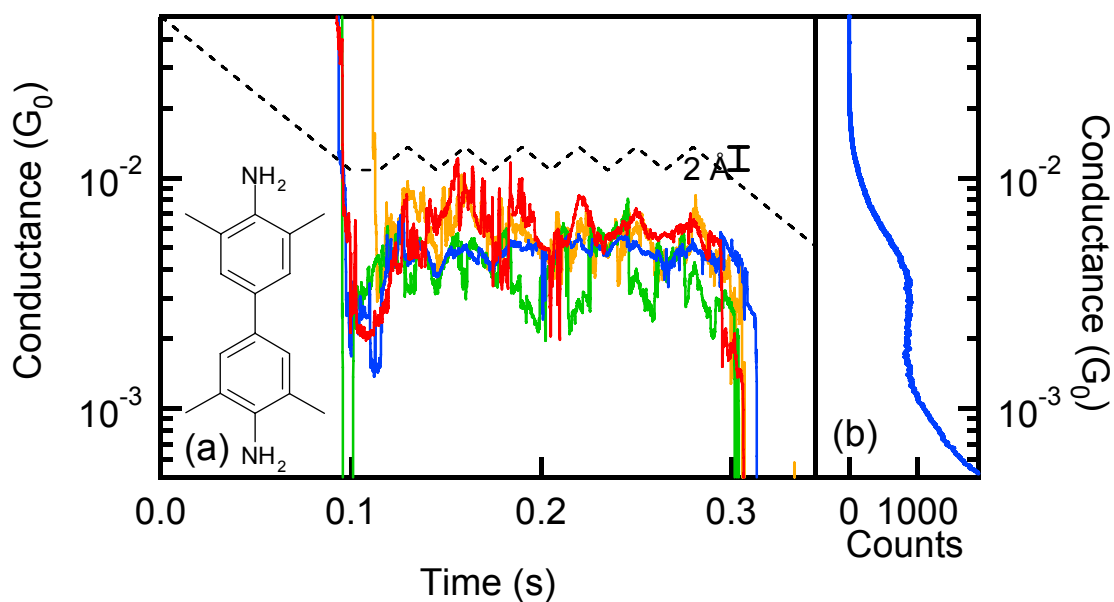
Switching Measurement Controls: Control measurements are performed using the same ramps in solvent alone and a solution of 3,3',5,5' Tetramethyl 4,4'Diamino Biphenyl;

neither showed a bimodal histogram indicative of switching (SI Figs. 3 and 4). Moreover, we find that switching in Au-bipyridine-Au junctions occurs reproducibly only if the ramp displacement amplitude is between ~ 2 Å and ~ 3 Å. Displacements larger than 3.5 Å break the junction. Displacements smaller than 2 Å were insufficient to switch between the low and high conducting states (SI Fig. 5). Control experiments with 2,4' bipyridine and 4-phenyl pyridine show no peak in the histogram (SI Fig. 1) indicating that strongly asymmetric junctions (bonded on one side only) or a configuration with pi-stacked molecular coordination^{11, 12} cannot explain either the Low G or High G configuration or the switching seen in these measurements.

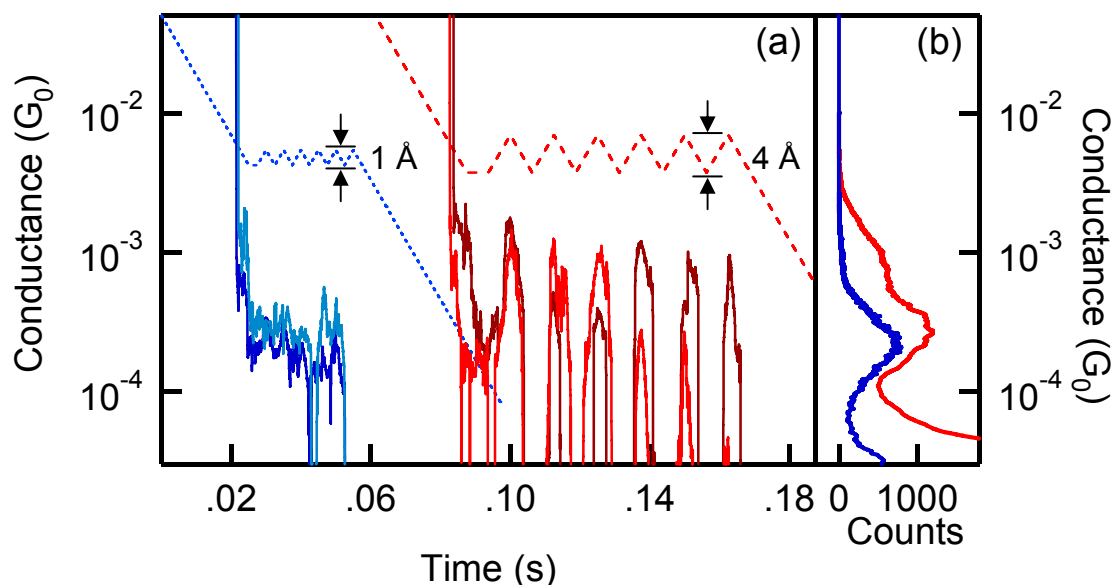
For measurements in solvent alone (SI Fig. 3), we used the same selection criteria, while for measurements with 3,3',5,5' Tetramethyl 4,4' Diamino biphenyl purchased from Sigma-Aldrich (SI Fig. 4), we required the hold section to start within the conductance peak observed for this molecule using our standard methodology. The histogram constructed from these selected traces measured in solvent alone (SI Fig. 3b) did not show any peak while that for 3,3',5,5' Tetramethyl 4,4'Diamino Biphenyl (SI Fig. 4b) showed a single peak around $4 \times 10^{-3} G_0$.



SI Fig. 3: (a) Sample switching traces measured with switching ramp (dashed line) in solvent alone (1,2,4 trichlorobenzene) showing conductance oscillations between varying conductances. (b) Conductance histogram constructed from ~500 selected traces out of 5000 measured traces. Measurements were carried at 250 mV.



SI Fig. 4: (a) Sample switching traces measured with zig-zag ramp (dashed line) in 3,3',5,5' tetramethyl 4,4' diaminobiphenyl (structure shown). (b) Conductance histogram constructed from ~500 selected traces out of 5000 measured traces measured at 250 mV.

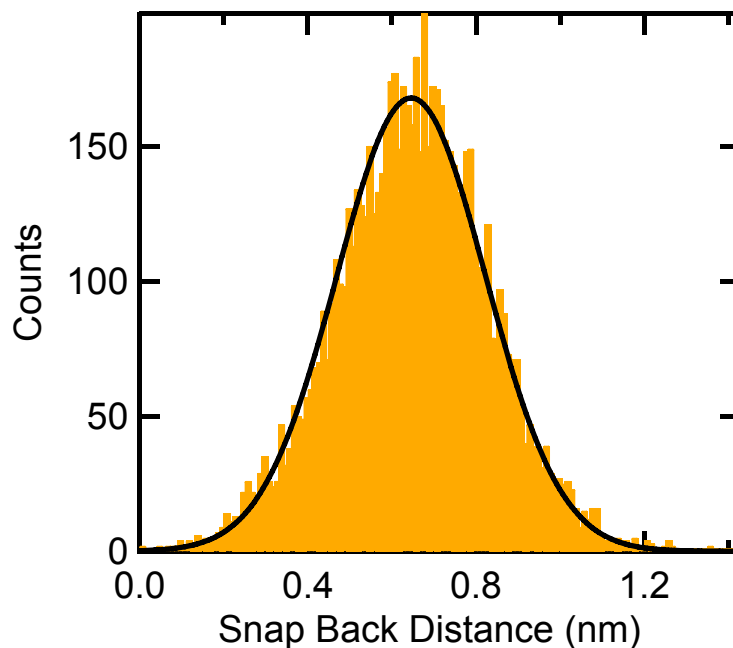


SI Fig. 5: (a) Sample 4,4' bipyridine switching traces (dark blue, light blue and red and brown) measured with zig-zag ramps with 1 Å amplitude (blue dashed line) and 4 Å amplitude (red dashed line). Note: Red traces are laterally offset by 0.06 s. (b) Conductance histogram constructed from ~ 200 selected traces out of 2000 measured traces measured at 250 mV. Blue histogram is for traces measured with 1 Å ramp, and shows a single peak at the Low G range. Red histogram is for traces measured with 4 Å ramp.

Control measurements were also run in 4,4' bipyridine using a zig-zag switching ramp with a displacement amplitude of 0.75 Å, 1 Å, 3 Å, 4 Å, and 5 Å. With a 3 Å amplitude, the switching traces and accompanying histograms looked very similar to those with a 2 Å amplitude ramp. For the 0.75 Å and 1 Å ramp, ~ 80% of the selected traces did not switch from the Low G starting value to the High G value (as shown in SI Fig. 5, blue traces). A few trace switched to the High G value and then remained at the high conductance until the junction was broken. For the 4 Å and 5 Å ramps, the junction was broke during the ramp and frequently reformed as shown in SI Fig. 5 (red traces).

Measurement of Au Snap Back Distance: When the gold-gold contact breaks, and no molecules are present, the Au atoms snap back³ leaving two electrodes that are not in contact. To determine the electrode separation soon after the Au contact is broken, we

push the electrodes back together until a conductance above $1 G_0$ is obtained, using a Piezo ramp similar to the one shown in Fig. 2c of the main text, but without the 0.05 s hold section. The distance that the electrodes need to be moved to form a contact is a measure of how much the atoms snap back when the junction is broken. A histogram of snap back distances is shown in SI Fig. 6, with a Gaussian fit that gives a mean snap back distance of 0.65 nm, in good agreement with measurements done in ultra high vacuum³.



SI Fig. 6: Distance that two gold electrodes need to be moved back to make a contact with conductance greater than $0.5 G_0$ after being pulled apart from a point-contact.

Theoretical Methods

Our density-functional calculations are performed using the generalized gradient approximation (GGA),⁴ as implemented in the SIESTA code.⁵ An optimized single- ζ basis set is used for the Au d shell; all other orbitals are described by double- ζ polarization basis sets. To check the basis set convergence, we computed the Au(111) work function and the frontier molecular levels for bipyridine on a trimer on Au(111), and compared our results with plane-wave calculations using the VASP⁶ package; excellent agreement, within 0.1 eV, was achieved for orbital energies and the Au(111) work function. Geometry optimization was performed by relaxing all atoms in the molecule, and Au atoms up to and including the third layer from either surface, until the forces on them are < 0.05 eV/Å. Γ -point sampling is sufficient for accurate geometry optimizations; binding energies are obtained with a $2 \times 2 \times 1$ Monkhorst-Pack \mathbf{k} -point mesh.

The conductance is obtained using a coherent elastic scattering state approach based on DFT.⁷ The junction is divided into three regions: left bulk, center resistive region (4 Au layers on either side of molecule), and right bulk. The center region is chosen large enough for the Hartree potentials at its boundaries to smoothly match those of the bulk. The bulk regions are infinitely repeated away from the junction to simulate open boundary conditions. Energy- and \mathbf{k}_{\parallel} -dependent scattering states are constructed with incoming and outgoing itinerant and evanescent states determined from the bulk Au complex band structure. Typical energy grid spacings used in this work are 10 meV. A 4×4 Monkhorst-Pack \mathbf{k}_{\parallel} -mesh is used sample the two-dimensional Brillouin zone; this is sufficient for convergence of the conductance and transmission function $T_{DFT}(E)$ in

bipyridine-Au junctions. The linear response DFT conductance is obtained from the Landauer formula ($G_{DFT} = T_{DFT}(E_F)G_0$).

The above DFT calculations enable the relatively efficient exploration of structure-conductance relationships. However, self-energy corrections to the molecular levels are required to obtain a more accurate conductance estimate.⁸ The self-energy correction Σ is applied using the procedure in Reference 8, which results in good agreement with experiment. To summarize the procedure, Σ is first estimated in two steps: (1) the electron affinity is calculated for the gas-phase molecule (using the Gaussian program with B3LYP exchange-correlation functional and 6-311g++dp basis set)⁹, resulting in a gas-phase correction of ~ 2.1 eV to the Kohn-Sham LUMO eigenvalue; (2) the gas-phase correction is modified by accounting for electrode polarization in the junction using an image charge model that assumes the electrodes are perfect conductors¹⁰ and includes an infinite series of images on either side of the junction. This change in Σ relative to gas phase, which we denote as W , represents the stabilization energy provided by screening in the Au electrodes for an electron added to the LUMO in the junction. To estimate W , we represent the electron in the LUMO as a point charge mid-way between the two image planes, which are taken to be 1 \AA from the Au(111) surface on either side of the junction.¹⁰ This gives $W = -\frac{e^2}{2a} \ln 2$, where a is the distance between the point charge and the image planes. We have found that replacing the point charge model with one involving Mulliken populations at the atomic positions of the molecule does not change W by more than 0.1 eV. Furthermore, changing the image plane position by about 1 \AA also results in only ~ 0.1 eV change in W . The calculated Σ in the junctions reported here varies from ~ 0.9 to 1.5 eV, depending on how close the molecule is to the electrodes. The

Σ -corrected conductance G is calculated with a Lorentzian fit

$$T_{Lor}(E) = \frac{\Gamma_1 \Gamma_2}{(E - E_R)^2 + \left(\frac{\Gamma_1 + \Gamma_2}{2}\right)^2}$$

to the DFT-based transmission function $T_{DFT}(E)$, and

applying the correction Σ to the resonance peak position E_R in the junction:

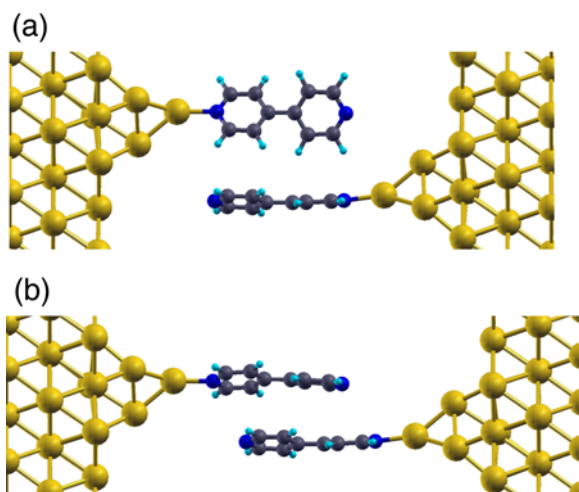
$$T(E) = \frac{\Gamma_1 \Gamma_2}{(E - (E_R + \Sigma))^2 + \left(\frac{\Gamma_1 + \Gamma_2}{2}\right)^2}, \quad G = T(E_F)G_0.$$

Our approximate self-energy

correction Σ is valid here since the bipyridine LUMO wavefunction in the junction is not significantly different from that in the gas-phase. We also assume that the width of the resonance does not change significantly when the LUMO peak is moved – this has been verified by calculations that apply the self-energy correction to the Hamiltonian governing the scattering state solutions. Finally, we have also checked that the correction Σ changes by only ~ 0.1 eV if our model flat surfaces are replaced by Au mounds with large radius of curvature $R \sim 50$ Å (expected for a soft metal like Au).

Discussion of Alternative Explanations for High G and Low G Configurations

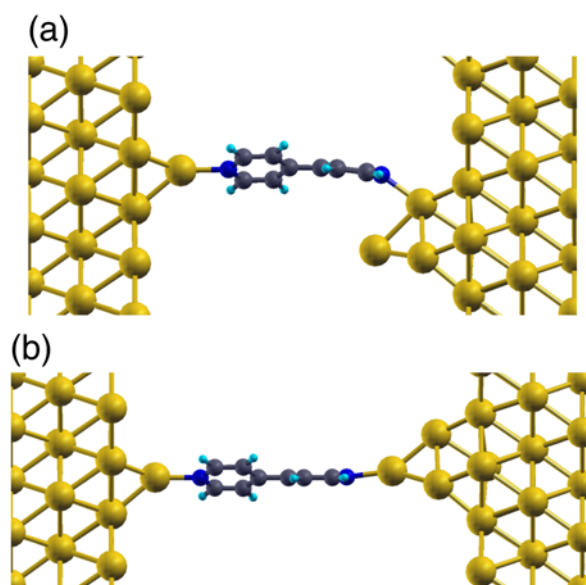
The calculations and experiments presented in the text show that the switching mechanism is based on changes in the N-Au contact geometry. We now provide evidence that rules out other mechanisms for switching in this system. Two alternative classes of mechanisms are considered: (a) mechanisms in which the low G geometry corresponds to junctions where the molecule is covalently bound to Au only at one end of the junction (Mechanism 1); (b) mechanisms that involve switching between different types of ‘near-vertical’ geometries (Mechanisms 2-4).

**SI Fig. 7**

Mechanism 1. We have considered the possibility that the high G geometry corresponds to junctions with a molecule bonded to both electrodes, while the low G geometry corresponds to junctions with two molecules, each bonded to only one electrode, and interacting with each other electrostatically/through π -stacking. SI Fig. 7a-b show these low G geometries, which are based on published work^{11, 12}. The calculated conductances are $1.7 \text{ E-}6$ and $2.0 \text{ E-}5 \text{ G}_0$ respectively, which are smaller than/comparable to the calculated conductances for broken junctions ($2\text{-}8 \text{ E-}5 \text{ G}_0$). Furthermore, conductance histograms for 2,4'-bipyridine and 4-phenyl pyridine have no peaks within the conductance range of 4,4'-bipyridine (SI Fig. 1), indicating that binding through N to both electrodes is required to form a stable junction with a conductance in this range.

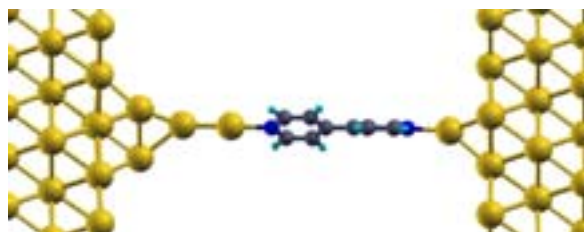
**SI Fig. 8**

Mechanism 2. Another possibility we have considered is that the low G peak comes from geometries in which the Au adatom is pulled to a less favorable atop (SI Fig. 8) or bridge site. However, the conductance of these junctions is of order $10^{-5} G_0$, comparable to those for broken junctions.



SI Fig. 9

Mechanism 3. We have also explored the possibility that the decrease in conductance from high to low G is due to a shift in binding site from the bottom of a pyramid-like motif to the tip of the pyramid – both geometries being ‘near-vertical’. The calculations indicate that binding to the tip instead results in a larger conductance (Fig. 3a: $1.54 \times 10^{-4} G_0$, Fig. 3b: $2.12 \times 10^{-4} G_0$), which may be related to the general trend of increasing conductance with decreasing coordination of the Au binding site.¹³



SI Fig. 10

Mechanism 4. Finally, we have considered the geometry in SI Fig. 10, where a ‘neck’ of Au atoms forms. Such Au necks would be feasible for thiol-Au junctions, where the strong S-Au bond pulls Au along with it. The weaker N-Au bonding would *not* support these geometries. Nonetheless, as a hypothetical construct, we have calculated the conductance of such a junction, which we find to be $2.24 \times 10^{-5} G_0$, comparable to that of broken junctions.

References

1. Ulrich, J. et al. Variability of Conductance in Molecular Junctions. *Journal of Physical Chemistry B* 110, 2462-2466 (2006).
2. Venkataraman, L. et al. Single-Molecule Circuits with Well-Defined Molecular Conductance. *Nano Letters* 6, 458 - 462 (2006).
3. Yanson, A. I., Bollinger, G. R., van den Brom, H. E., Agrait, N. & van Ruitenbeek, J. M. Formation and manipulation of a metallic wire of single gold atoms. *Nature* 395, 783-785 (1998).
4. Perdew, J. P., Burke, K. & Ernzerhof, M. Generalized gradient approximation made simple. *Physical Review Letters* 77, 3865-3868 (1996).
5. Soler, J. M. et al. The SIESTA method for *ab initio* order- N materials simulation. *Journal of Physics-Condensed Matter* 14, 2745-2779 (2002).
6. Kresse, G. & Furthmuller, J. Efficient iterative schemes for *ab initio* total-energy calculations using a plane-wave basis set. *Phys. Rev. B* 54, 11169 (1996).
7. Choi, H. J., Marvin, L. C. & Steven, G. L. First-principles scattering-state approach for nonlinear electrical transport in nanostructures. *Physical Review B (Condensed Matter and Materials Physics)* 76, 155420 (2007).
8. Quek, S. Y. et al. Amine-Gold Linked Single-Molecule Junctions: Experiment and Theory. *Nano Letters* 7, 3477-3482 (2007).
9. Frisch, M. J. et al. Gaussian 03, Revision C.02. Gaussian, Inc., Wallingford CT, 2004.
10. Neaton, J. B., Hybertsen, M. S. & Louie, S. G. Renormalization of molecular electronic levels at metal-molecule interfaces. *Physical Review Letters* 97, 216405 (2006).
11. Emberly, E. G. & Kirczenow, G. Theoretical study of electrical conduction through a molecule connected to metallic nanocontacts. *Physical Review B* 58, 10911-10920 (1998).
12. Wu, S. M. et al. Molecular junctions based on aromatic coupling. *Nature Nanotechnology* 3, 569-574 (2008).
13. Stadler, R., Thygesen, K. S. & Jacobsen, K. W. Forces and conductances in a single-molecule bipyridine junction. *Physical Review B* 72, 241401 (2005).